

Absence of hydrogen bonding in charge-ordered organic conductor α -(BEDT-TTF) $_2$ I $_3$ probed by ^{127}I -NQR

T. Kobayashi,^{1,2,3,*} Y. Kato,¹ H. Taniguchi,¹ T. Tsumuraya,⁴ K. Hiraki,⁵ and S. Fujiyama³

¹Graduate School of Science and Engineering, Saitama University, Saitama, 338-8570, Japan

²Research and Development Bureau, Saitama University, Saitama 338-8570, Japan

³Meson Science Laboratory, RIKEN, Saitama 351-0198, Japan

⁴POIE, Kumamoto University, Kumamoto 860-8555, Japan

⁵Center for Integrated Science and Humanities, Fukushima Medical University, Fukushima, 960-1295, Japan

(Dated: August 15, 2022)

We present ^{127}I nuclear quadrupole resonance spectra and nuclear relaxation of α -(BEDT-TTF) $_2$ I $_3$ that undergoes a charge ordering transition. Only one of the two I $_3$ anion sites shows a significant differentiation in the electric field gradients across the first order transition, which shows that the anion-donor hybridization through hydrogen bonding is a secondary contribution to the charge ordering. The dominating source for the nuclear relaxation is the local libration of the I $_3$ anions, but an anomalous peak is detected just below the transition, as observed by ^{13}C NMR.

Hydrogen bonding, an attractive interaction between protons and electronegative atoms, provides unique physical properties for materials such as water ice, soft matter systems, and organic compounds. However, the effects of hydrogen bonding on electronic or magnetic materials have not been clarified. The main causes of this are twofold. One reason is theoretical, such that suitable models cannot be obtained due to the motion of the hydrogen atoms. The other reason is experimental, because x-ray diffraction is insensitive to the hydrogen atoms, and NMR cannot discriminate between protons at multiple positions in the crystal lattice. Still, hydrogen bonding plays a crucial role in several unique properties of molecular solids. For example, emergent ferroelectricity has been realized in single-component molecular crystals associated with the quantum Berry phase [1–3], and the magnetic ordering can be suppressed by the anharmonic motion of hydrogen between two molecules, resulting in quantum spin liquid-like behavior [4–6]. These two example materials have a large charge gap, but the effect of hydrogen bonding in conducting molecular solids on the Fermi surface remains unclear.

A quasi-two-dimensional organic conductor, α -(BEDT-TTF) $_2$ I $_3$ (where BEDT-TTF is bis(ethylenedithio)tetrathiafulvalene, hereafter abbreviated as ET), shown in Fig. 1(a), is one of the most studied organic conductors [7]. This material has a 3/4-filled (1/4-filled hole) electronic band, showing a Mott-insulating instability. One prominent property of α -ET $_2$ I $_3$ is the realization of a Dirac electron system under applied pressure [8–12]. At the ambient pressure, the system shows a metal-insulator transition at $T \approx 135$ K associated with a charge ordering (CO) [13–15]. It is widely accepted that the modulation pattern of the CO is not checkerboard-like but zig-zag-chain-like with charge-rich sites A and B, and charge-poor sites A' and C (Fig. 1(b)), as revealed by x-ray structural analysis

[16], infrared and Raman spectroscopy [17–19], and ^{13}C -NMR spectroscopy [20–23].

Despite the consensus on the modulation pattern, issues remain regarding the mechanism of the CO transition. Many theoretical studies have been conducted and a variety of proposals have been made. Coulomb repulsion in the quarter-filled band of the ET layers has been proposed [24–28], followed by a claim that electron-phonon interaction plays a crucial role to reproduce the CO pattern [29–32]. While these theories consider only interactions within the intra-ET layers, some approaches actively incorporate the role of the anion layer through hydrogen bonding. Reference [33] pointed out the significant role of the H-I $^{-1/2}$ σ -bond between the anion and edge protons in the ET molecule. Since the energy difference between the σ -bond and π -electrons of donor molecules are far apart, the σ hybridization is not expected to directly cause CO. However, even if it is an indirect contribution, the problem regarding the stability of the Mottness of the quarter-filled band perturbed by the hydrogen bond attracts much attention.

In this letter, we propose ^{127}I -nuclear quadrupole resonance (NQR) as a microscopic tool to examine the specific H-I $^{-1/2}$ bonds, which has never been applied to organic conductors. The NQR spectra of α -ET $_2$ I $_3$ are quantitatively reproduced using first-principles calculations, which enables us to claim the microscopic interactions that occur during the CO transition. Utilizing another merit of NQR, unlike with ^{13}C NMR, we can directly observe static and dynamic charge properties via an electric field gradient (EFG), and we found the zig-zag-like charge modulation in the CO state across a first-order transition. Long-range electrostatic interaction from the ET layer is the first source, and the local hydrogen bonding between the I $_3$ anions and ET molecules is a secondary source to split NQR spectral lines. The nuclear spin-lattice relaxation rate ($1/T_1$) is dominated by local fluctuation of the I $_3$ anions, of which the energy is five times smaller than the Debye frequency. We also found enhancements of $1/T_1$ just below the CO transition

* tkobayashi@phy.saitama-u.ac.jp

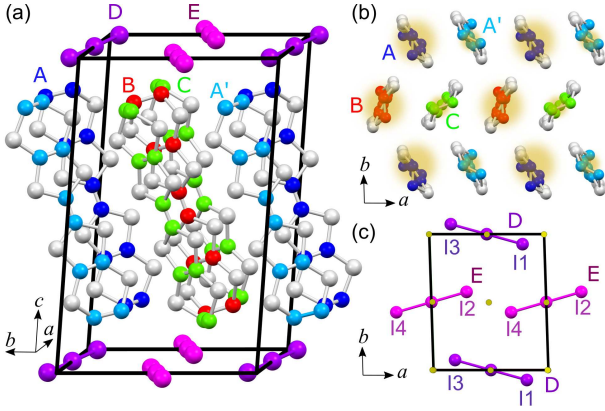


FIG. 1. Crystal structure of (a) α -I₃ [34]. BEDT-TTF molecules labeled as A, B (A', C) show charge rich (poor) sites for $T > T_{CO}$. (b) Top view of the conduction plane in the CO state. (c) Insulating I₃ plane. The inversion center is lost for $T < T_{CO}$, by which I1 and I3, and I2 and I4 sites become crystallographically inequivalent.

temperature, T_{CO} .

Single crystals of α -ET₂I₃ were grown by the standard electrochemical reaction [13]. The ¹²⁷I-NQR experiment was performed on a polycrystalline sample of 14.2 mg under zero magnetic fields. The NQR spectrum was obtained by fast Fourier transformation of the spin-echo signal with a $\pi/2$ - π pulse sequence, where the typical $\pi/2$ pulse length was 2.5 μ s. The $1/T_1$ were measured using the inversion and saturation recovery methods and were obtained by fitting the magnetization curves using $1 - M(t)/M(\infty) \propto 3/28 \exp(-3t/T_1) + 25/28 \exp(-10t/T_1)$. Here, t is the interval between inversion (saturation) and the first $\pi/2$ pulses, and $M(t)$ is the magnetization at time t . We confirmed that the same T_1 values were obtained by both methods in the appropriate temperature range. EFGs at the iodine sites of α -ET₂I₃ were calculated using the first-principles calculations based on the full-potential linearized augmented plane wave (FLAPW) method [35, 36]. The calculation are based on the density-functional theory (DFT), and the exchange and correlation potential is represented by a generalized gradient approximation in the Perdew-Burke-Ernzerhof formula [37]. (See the Supplemental Material [38]).

We found two ¹²⁷I-NQR spectral lines at 172.2 and 173.1 MHz at 150 K, as shown in Fig. 2(a), while sweeping in the range of 170–176 MHz. Reported ¹²⁷I-NQR studies of I₃ anions in quaternary ammonium salts indicated that the observed resonances are ascribed to $\pm 1/2 \leftrightarrow \pm 3/2$ transitions of the terminal iodines [39, 40]. At a terminal iodine, the EFG tensor is nearly axially symmetric [40] (i.e., $\eta = (V_{xx} - V_{yy})/V_{zz} \simeq 0$, where V_{ii} ($i = x, y, z$) are the diagonal components of the EFG tensor). The NQR frequency, ν_Q , is expressed as $\nu_Q = \frac{3eQV_{zz}}{20h} (1 + \frac{59}{54}\eta^2)$, where e , Q , and h are the elementary charge, the nuclear quadrupole moment of ¹²⁷I nucleus

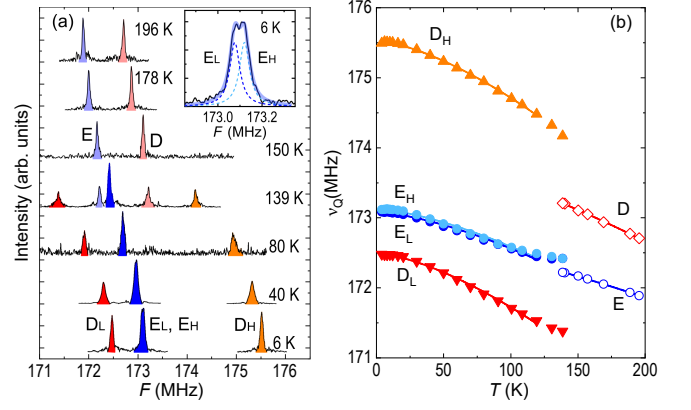


FIG. 2. (a) Temperature evolution of the ¹²⁷I-NQR spectra. The inset shows the central peak at 6 K. (b) Temperature dependence of the ¹²⁷I-NQR frequency. The solid lines are the fitting curves of $\nu_Q(T) = \nu_0(1 - \alpha T^{3/2})$.

(−680(10) mb [41]), and Planck’s constant, respectively.

In α -ET₂I₃, two crystallographically independent I₃ anions, D and E, exist (Fig. 1(c)). Since the central iodine of each anion is located at the inversion center (1c and 1d sites in Wyckoff positions), the terminal iodines of each anion group are equivalent and occupied at $2i$ sites above T_{CO} . As a result, two independent terminal iodines exist, holding relations I1 = I3 and I2 = I4 (‘=’ denotes the site equivalency), which agrees with the two distinct lines observed in our NQR spectra. As discussed below, the signals at the high and low frequencies can be assigned to the D and E sites, respectively, from the calculation of the EFG using first-principles method.

At 139 K, five distinct lines are observed, as shown in Fig. 2(a), and the three new lines remain down to the lowest temperature. The temperature of 139 K corresponds to T_{CO} , and the coexistence of high-temperature and low-temperature peaks in the spectrum indicates a first-order transition. Below T_{CO} , four spectra are expected according to the loss of the inversion center by the CO transition [16]. Although the number of observed signals below T_{CO} is three, the signal intensities are approximately 1:2:1 from the low-frequency side, suggesting that the NQR signals consist of four sites. The central peak below T_{CO} splits slightly, as shown in the inset of Fig. 2(a). We considered that two sites overlap at $\nu_Q \approx 173$ MHz because they exhibit nearly the same magnitude of EFG at the terminal iodine sites.

All the ν_Q s increase upon cooling as a result of lattice contraction, as shown in Fig. 2 (b). The slope of ν_Q at the D site is larger than that at the E site above T_{CO} , and below T_{CO} , the slopes of ν_Q at the high- and low-frequency signals are larger than that at the central frequency. An empirical formula for temperature-dependent $\nu_Q(T)$ considering thermal expansion of the unit cell, $\nu_Q(T) = \nu_0(1 - \alpha T^{3/2})$ [42], fits the experiments well (solid lines in Fig. 2(b)), and we summarize the fit-

TABLE I. Fitted parameters obtained by fitting $\nu_Q(T)$ at each site with $\nu_Q(T) = \nu_0(1 - \alpha T^{3/2})$.

	ν_0 (MHz)	α ($K^{-3/2}$)
D	$T > T_{CO}$	173.94(1)
	$T < T_{CO}$	172.493(6)
		175.528(4)
E	$T > T_{CO}$	172.72(1)
	$T < T_{CO}$	173.081(7)
		173.123(9)

ted parameters in Table I. Comparing α values, α at the D site is 1.5 times larger than at the E site above T_{CO} , and α at the two outer lines is also 1.5 times larger than at the central line below T_{CO} . Thus, we concluded that the two outer lines originate from the D anion (hereafter, we refer to them as D_H and D_L), and the overlapped central line originates from the E anion (E_H and E_L). These results show that ν_Q of the D site changes significantly because of the CO transition, whereas the change in ν_Q of the E site is negligible.

We calculated the EFG at each iodine position using the FLAPW method to clarify the relationship between the measured NQR signals and the actual iodine positions [38]. Since the EFG is usually very sensitive to internal atomic coordinates [43] and hydrogen atom positions determined from x-ray diffraction were not so accurate [44], we performed structural optimization for iodine and hydrogen atom positions. The relaxed structures with the CIF format are included in the Supplemental Material [38]. At 150 K, the calculations show that $\nu_Q = 174.0$ MHz at the D site, which is 0.4 % larger than $\nu_Q = 173.3$ MHz at the E site. Experimentally, the difference in frequency between the two NQR lines is approximately 0.5 %, which is in good quantitative agreement. Hence, the high- and low- frequency lines are interpreted as signals originating from D and E anions.

At 30 K, the calculated ν_Q at the D site splits significantly into two lines with higher and lower frequencies, while the change at the E site is small. To discuss the amount of change in the D and E sites during the CO transition, we define $(\Delta\nu/\nu)_{Q,k} \equiv \frac{(\nu_{Q,k_H} - \nu_{Q,k_L})_{30K}}{(\nu_{Q,k})_{150K}}$ ($k = D, E$ sites), resulting in experimental values: $(\Delta\nu/\nu)_{Q,D} = 1.75$ % and $(\Delta\nu/\nu)_{Q,E} = 0.02$ %; calculated values: $(\Delta\nu/\nu)_{Q,D} = 0.74$ % and $(\Delta\nu/\nu)_{Q,E} = 0.19$ %. The first-principles DFT calculations qualitatively explain the experimental results well, including the CO transition. Our evaluation of ν_Q using the first-principles calculation suggests that it provides useful predictions for conducting NQR experiments on organic conductors.

The NQR frequency, ν_Q , solely depends on the bond length between the central and terminal iodines of the I_3 molecule; however, the charge modulation in the ET layer also affects the ν_Q and splits the line for the D site. In Fig. 3(a), we show the positions of the iodines and the middle positions of the central C=C bond of the ET molecules. As for the D anion, two A ET molecules

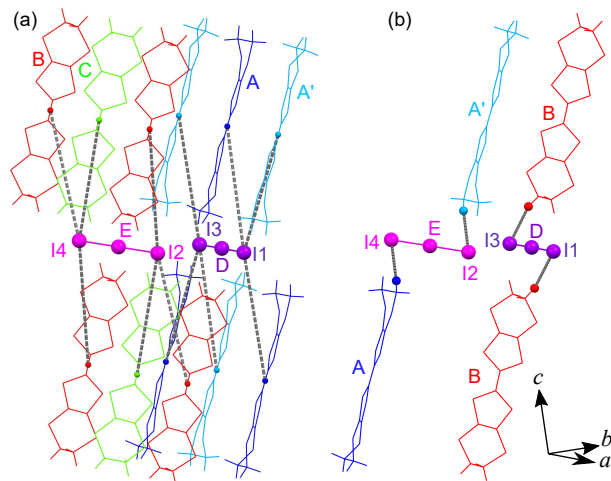


FIG. 3. Geometrical relations between the iodines and ET molecules in the CO state. (a) ET molecules relevant to each iodine assuming long-range electronic interactions as a source to split the NQR line of the D site. Dashed lines denote direct paths from the central position of the C=C central bond of each ET molecule and iodine spacing shorter than 9 Å. (b) Potential terminal protons of ET molecules composing H-I^{-1/2} bonds at the shortest distance from each terminal iodine (< 3 Å).

and one A' are located near I1, while one A and two A' molecules are close to I3. This results in different EFGs between I1 and I3. On the other hand, both I2 and I4 at E anion are close to two B molecules and one C molecule, which causes no significant difference in the EFGs. This argument is consistent with our observations. Reference [33] argues that the H-I^{-1/2} hybridization between the I₃⁻¹ anions and edge protons in ET molecules is the crucial source of the CO. As shown in Fig. 3(b), potential protons that hybridize with both I1 and I3 are equally the edge protons of B molecules. As for the E anion, protons of A'(A) molecules can hybridize with I2(I4). This geometrical argument suggests a significant splitting of line E and negligible splitting of D, which is inconsistent with the experiments. We concluded that the line splitting of D originates from long-range interactions from the charge-ordered ET layer and is not mediated by local H-I^{-1/2} hybridization.

In Fig. 4, we show the temperature-dependent nuclear spin-lattice relaxation rate, $1/T_1$, for each spectral line. No significant variation in $1/T_1$ for the distinct lines is observed. The $1/T_1$ nearly follows power relations in regards to temperature, $1/T_1 \propto T^\beta$, which differs from ¹³C NMR [23]. The β changes from high-temperature, $\beta = 2$, to low-temperature, $\beta \approx 7$, suggesting that the relaxation mechanism is quadrupolar relaxation of nuclei by two-phonon Raman processes [45, 46]. The $1/T_1$

originating from this process is expressed as [47],

$$\left(\frac{1}{T_1}\right)_Q \simeq \frac{81\pi}{2} \left(\frac{F_2\hbar}{mv^2}\right)^2 \int_0^\Omega \frac{e^{\hbar\omega/k_B T}}{(e^{\hbar\omega/k_B T} - 1)^2} \left(\frac{\omega}{\Omega}\right)^6 d\omega, \quad (1)$$

where k_B, m, Ω are the Boltzmann constant, the mass of the ^{127}I nucleus, and a cutoff frequency, respectively. v is the sound velocity in the crystal, which is an order of 10^3 m/s in organic conductors [48]. Ω is represented by the temperature $\Theta = (\hbar/k_B)\Omega$ and can be estimated as the Debye temperature, $\Theta = \Theta_D = 200$ K, which is obtained by heat capacity measurements of ET organic conductors. F_2 characterizes the phonon modulation of the EFG and is difficult to determine precisely; however, the simplest estimate, $F_2 = 2\pi\nu_Q$, works well [46, 49].

The calculated $(1/T_1)_Q$ is plotted as the blue dashed line in Fig. 4 using $\nu_Q = 173$ MHz and $\Theta = 200$ K, which is significantly smaller than the experimental $1/T_1$. Instead, the calculated $(1/T_1)_Q$ using $\Theta = 45$ K (green dashed line) reproduces the experiments well. This discrepancy suggests that the local Θ at iodine sites in Eq. (1) can be smaller than the global Debye temperature, Θ_D , estimated from macroscopic measurements. We can cite several related experiments. The ^{129}I -Mössbauer results of $\beta\text{-ET}_2\text{I}_3$ have been explained using the local Debye temperature of ~ 100 K [50], which is smaller than $\Theta_D \simeq 200$ K estimated from the heat capacity measurement [51]. Raman spectra also showed a low-lying molecular vibration mode with 27 cm^{-1} ($= 38$ K) assigned to libration of I_3 anions, a reciprocating motion with a fixed position in the middle of the I_3 ‘stick’ (i.e. the central iodine). These arguments are consistent with our observations.

Around the T_{CO} , we found small peaks for $1/T_1$ of the charge-sensitive D_H and D_L lines, as shown in the inset of Fig. 4. Notably, that the peak temperature is located just below T_{CO} , by which we consider the source for the additional relaxation is not a critical slowing down for the CO. A similar peak for $1/T_1$ just below the T_{CO} was observed by ^{13}C -NMR for the charge-rich site [23]. Reference [23] argues that an emergent antiferromagnetic zig-zag chain ($S = 1/2$) for $T < T_{\text{CO}}$ that undergoes a singlet state with a sizable gap of $\Delta = 40$ meV [28]. We plot $1/T_1 = (1/T_1)_Q + \text{const.} \times \exp(-\Delta/k_B T)$ as the solid lines in the inset of Fig. 4 and find good agreements with the experimental $1/T_1$ for the D_H and D_L sites. However, we cannot conclude that magnetic fluctuation from charge-ordered ET layers is the source for the peaks of $1/T_1$ because $1/T_1$ for D_H and D_L sites that are close to charge-rich and poor ET molecules show comparable enhancements.

When we consider the difference in the relaxation mechanisms of ^{13}C and ^{127}I (i.e., magnetic fluctuation of the local spin density for the former and EFG fluctuation for the latter), we can point out another possibility, other than an emergent spin chain that undergoes a spin-singlet state. In charge-density-wave (CDW) systems, it is argued that coherence peak-like properties just below

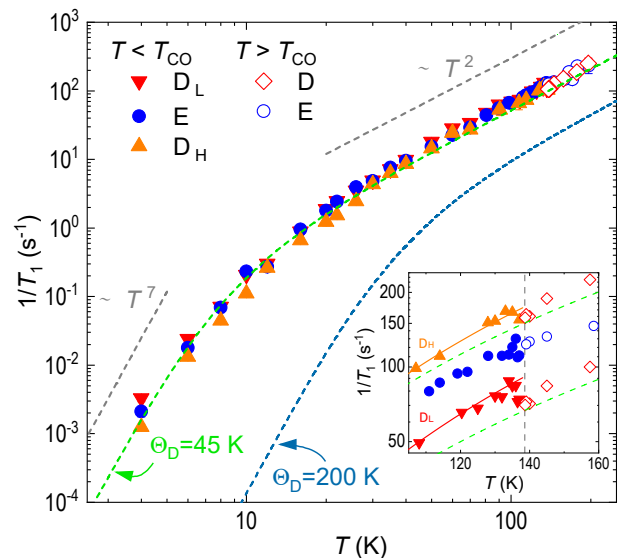


FIG. 4. Temperature dependence of $1/T_1$. The dashed lines are calculated $(1/T_1)_Q$ with $\Theta = 45$ K and 200 K. The inset shows the temperature dependence of $1/T_1$ in the vicinity of T_{CO} . For clarity, the D_H and D_L data are multiplied and divided by 1.5, respectively. The solid curves are $1/T_1 = (1/T_1)_Q + \text{const.} \times \exp(-\Delta/k_B T)$.

the transition temperature can emerge, originating from singularity of the density of states across the CDW gap [52–54]. The electron density is also expected to follow an activated T dependence; then, we cannot discriminate between the energy gaps in the CDW and spin-singlet Mott systems. The first-principles calculations also show a similar singularity for the gap opening due to Coulomb repulsion [6, 55]. Detailed theoretical analyses considering the gap structures and the relationships between the magnitudes of the gap and leading electronic/magnetic interactions are necessary to determine the origins of the gap.

In summary, we obtained ^{127}I -NQR spectra and $1/T_1$ for $\alpha\text{-ET}_2\text{I}_3$ that undergoes a CO transition at ambient pressure. The first-principles calculations accurately reproduced the NQR frequency of each spectral line, which enabled us to examine the microscopic interactions. Significant splitting of the spectral line of the D site indicates that the H-I $^{-1/2}$ bond is a secondary source for the CO. Furthermore, $1/T_1$ is predominantly determined by a two-phonon process characterized by local vibration of I_3 anions. The charge order phase transition is first-order, without critical slowing down of the electronic charges. Just below the T_{CO} , $1/T_1$ shows an additional relaxation similar to the reported ^{13}C NMR.

ACKNOWLEDGMENTS

We are grateful to H. Sawa and H. Seo for their helpful discussions. This work was partially supported by the

-
- [1] S. Horiuchi, F. Ishii, R. Kumai, Y. Okimoto, H. Tachibana, N. Nagaosa, and Y. Tokura, Ferroelectricity near room temperature in co-crystals of nonpolar organic molecules, *Nature Materials* **4**, 163 (2005).
- [2] F. Ishii, N. Nagaosa, Y. Tokura, and K. Terakura, Covalent ferroelectricity in hydrogen-bonded organic molecular systems, *Physical Review B* **73**, 212105 (2006).
- [3] S. Horiuchi, Y. Tokunaga, G. Giovannetti, S. Picozzi, H. Itoh, R. Shimano, R. Kumai, and Y. Tokura, Above-room-temperature ferroelectricity in a single-component molecular crystal, *Nature* **463**, 789 (2010).
- [4] M. Shimozawa, K. Hashimoto, A. Ueda, Y. Suzuki, K. Sugii, S. Yamada, Y. Imai, R. Kobayashi, K. Itoh, S. Iguchi, M. Naka, S. Ishihara, H. Mori, T. Sasaki, and M. Yamashita, Quantum-disordered state of magnetic and electric dipoles in an organic mott system, *Nature Communications* **8**, 1821 (2017).
- [5] T. Isono, H. Kamo, A. Ueda, K. Takahashi, M. Kimata, H. Tajima, S. Tsuchiya, T. Terashima, S. Uji, and H. Mori, Gapless Quantum Spin Liquid in an Organic Spin-1/2 Triangular-Lattice κ -H₃(Cat-EDT-TTF)₂, *Physical Review Letters* **112**, 177201 (2014).
- [6] T. Tsumuraya, H. Seo, R. Kato, and T. Miyazaki, First-principles study of hydrogen-bonded molecular conductor κ -H₃(Cat-EDT-TTF/ST)₂, *Physical Review B* **92**, 035102 (2015).
- [7] M. Dressel and S. Tomić, Molecular quantum materials: electronic phases and charge dynamics in two-dimensional organic solids, *Advances in Physics* **69**, 1 (2020).
- [8] N. Tajima, M. Tamura, Y. Nishio, K. Kajita, and Y. Iye, Transport Property of an Organic Conductor α -(BEDT-TTF)₂I₃ under High Pressure - Discovery of a Novel Type of Conductor -, *Journal of the Physical Society of Japan* **69**, 543 (2000).
- [9] S. Katayama, A. Kobayashi, and Y. Suzumura, Pressure-Induced Zero-Gap Semiconducting State in Organic Conductor α -(BEDT-TTF)₂I₃ Salt, *Journal of the Physical Society of Japan* **75**, 054705 (2006).
- [10] K. Kajita, Y. Nishio, N. Tajima, Y. Suzumura, and A. Kobayashi, Molecular Dirac Fermion Systems - Theoretical and Experimental Approaches-, *Journal of the Physical Society of Japan* **83**, 072002 (2014).
- [11] M. Hirata, K. Ishikawa, G. Matsuno, A. Kobayashi, K. Miyagawa, M. Tamura, C. Berthier, and K. Kanoda, Anomalous spin correlations and excitonic instability of interacting 2D Weyl fermions, *Science* **358**, 1403 (2017).
- [12] S. Fujiyama, H. Maebashi, N. Tajima, T. Tsumuraya, H.-B. Cui, M. Ogata, and R. Kato, Large diamagnetism and electromagnetic duality in two-dimensional dirac electron system, *Physical Review Letters* **128**, 027201 (2022).
- [13] K. Bender, I. Hennig, D. Schweitzer, K. Dietz, H. Endres, and H. J. Keller, Synthesis, Structure and Physical Properties of a Two-Dimensional Organic Metal, Di[bis(ethylenedithio)tetrathiofulvalene]triiodide, (BEDT-TTF)₂⁺I₃⁻, *Molecular Crystals and Liquid Crystals* **108**, 359 (1984).
- [14] K. Yamamoto, S. Iwai, S. Boyko, A. Kashiwazaki, F. Hiramatsu, C. Okabe, N. Nishi, and K. Yakushi, Strong Optical Nonlinearity and its Ultrafast Response Associated with Electron Ferroelectricity in an Organic Conductor, *Journal of the Physical Society of Japan* **77**, 074709 (2008).
- [15] S. Tomić and M. Dressel, Ferroelectricity in molecular solids: a review of electrodynamic properties, *Reports on Progress in Physics* **78**, 096501 (2015).
- [16] T. Kakiuchi, Y. Wakabayashi, H. Sawa, T. Takahashi, and T. Nakamura, Charge Ordering in α -(BEDT-TTF)₂I₃ by Synchrotron X-ray Diffraction, *Journal of the Physical Society of Japan* **76**, 113702 (2007).
- [17] R. Wojciechowski, K. Yamamoto, K. Yakushi, M. Inokuchi, and A. Kawamoto, High-pressure Raman study of the charge ordering in α -(BEDT-TTF)₂I₃, *Physical Review B* **67**, 224105 (2003).
- [18] T. Ivek, B. Korin-Hamzić, O. Milat, S. Tomić, C. Clauss, N. Drichko, D. Schweitzer, and M. Dressel, Electrodynamic response of the charge ordering phase: Dielectric and optical studies of α -(BEDT-TTF)₂I₃, *Physical Review B* **83**, 165128 (2011).
- [19] K. Yakushi, Infrared and Raman Studies of Charge Ordering in Organic Conductors, BEDT-TTF Salts with Quarter-Filled Bands, *Crystals* **2**, 1291 (2012).
- [20] Y. Takano, K. Hiraki, H. M. Yamamoto, T. Nakamura, and T. Takahashi, Charge disproportionation in the organic conductor, α -(BEDT-TTF)₂I₃, *Journal of Physics and Chemistry of Solids* **62**, 393 (2001).
- [21] S. Hirose and A. Kawamoto, Local spin susceptibility in the zero-gap-semiconductor state of α -(BEDT-TTF)₂I₃ probed by ¹³C NMR under pressure, *Physical Review B* **82**, 115114 (2010).
- [22] M. Hirata, K. Ishikawa, K. Miyagawa, K. Kanoda, and M. Tamura, ¹³C NMR study on the charge-disproportionated conducting state in the quasi-two-dimensional organic conductor α -(BEDT-TTF)₂I₃, *Physical Review B* **84**, 125133 (2011).
- [23] K. Ishikawa, M. Hirata, D. Liu, K. Miyagawa, M. Tamura, and K. Kanoda, Spin excitations in the quasi-two-dimensional charge-ordered insulator α -(BEDT-TTF)₂I₃ probed via ¹³C NMR, *Physical Review B* **94**, 085154 (2016).
- [24] H. Kino and H. Fukuyama, On the Phase Transition of α -(ET)₂I₃, *Journal of the Physical Society of Japan* **64**, 1877 (1995).
- [25] H. Kino and H. Fukuyama, Phase Diagram of Two-Dimensional Organic Conductors: (BEDT-TTF)₂X, *Journal of the Physical Society of Japan* **65**, 2158 (1996).
- [26] H. Seo and H. Fukuyama, Antiferromagnetic phases of one-dimensional quarter-filled organic conductors, *Journal of the Physical Society of Japan* **66**, 1249 (1997).
- [27] H. Seo, Charge Ordering in Organic ET Compounds, *Journal of the Physical Society of Japan* **69**, 805 (2000).
- [28] Y. Tanaka and M. Ogata, Correlation Effects on Charge Order and Zero-Gap State in the Organic Conductor α -(BEDT-TTF)₂X, *Journal of the Physical Society of*

- Japan **85**, 104706 (2016).
- [29] R. Torsten Clay, S. Mazumdar, and D. K. Campbell, Charge Ordering in θ -(BEDT-TTF)₂X Materials, *Journal of the Physical Society of Japan* **71**, 1816 (2002).
- [30] Y. Tanaka and K. Yonemitsu, Charge Order with Structural Distortion in Organic Conductors: Comparison between θ -(ET)₂RbZn(SCN)₄ and α -(ET)₂I₃, *Journal of the Physical Society of Japan* **77**, 034708 (2008).
- [31] S. Miyashita, Y. Tanaka, S. Iwai, and K. Yonemitsu, Charge, lattice, and spin dynamics in photoinduced phase transitions from charge-ordered insulator to metal in quasi-two-dimensional organic conductors, *Journal of the Physical Society of Japan* **79**, 034708 (2010).
- [32] M. Udagawa and Y. Motome, Charge Ordering and Coexistence of Charge Fluctuations in Quasi-Two-Dimensional Organic Conductors θ -(BEDT-TTF)₂X, *Physical Review Letters* **98**, 206405 (2007).
- [33] P. Alemany, J.-P. Pouget, and E. Canadell, Essential role of anions in the charge ordering transition of α -(BEDT-TTF)₂I₃, *Physical Review B* **85**, 195118 (2012).
- [34] S. Kitou, T. Tsumuraya, H. Sawahata, F. Ishii, K.-i. Hiraki, T. Nakamura, N. Katayama, and H. Sawa, Ambient-pressure Dirac electron system in the quasi-two-dimensional molecular conductor α -(BETS)₂I₃, *Physical Review B* **103**, 035135 (2021).
- [35] E. Wimmer, H. Krakauer, M. Weinert, and A. J. Freeman, Full-potential self-consistent linearized-augmented-plane-wave method for calculating the electronic structure of molecules and surfaces: O₂ molecule, *Physical Review B* **24**, 864 (1981).
- [36] J. Yu, A. J. Freeman, R. Podloucky, P. Herzig, and P. Weinberger, Origin of electric-field gradients in high-temperature superconductors: YBa₂Cu₃O₇, *Physical Review B* **43**, 532 (1991).
- [37] J. P. Perdew, K. Burke, and M. Ernzerhof, Generalized Gradient Approximation Made Simple, *Physical Review Letters* **77**, 3865 (1996).
- [38] See the Supplemental Material for detailed calculation of EFG.
- [39] Y. Yoshioka, N. Nakamura, and H. Chihara, On the correlation between NQR frequency and bond length in I₃⁻, *Journal of Molecular Structure* **111**, 151 (1983).
- [40] G. A. Bowmaker and S. Hacobian, Nuclear quadrupole resonance of charge transfer complexes. I. The trihalide ions, *Australian Journal of Chemistry* **21**, 551 (1968).
- [41] H. Yakobi, E. Eliav, L. Visscher, and U. Kaldor, High-accuracy calculation of nuclear quadrupole moments of atomic halogens, *The Journal of Chemical Physics* **126**, 054301 (2007).
- [42] J. Christiansen, P. Heubes, R. Keitel, W. Klinger, W. Loeffler, W. Sandner, and W. Witthuhn, Temperature Dependence of the Electric Field Gradient in Noncubic Metals, *Zeitschrift für Physik B Condensed Matter* **24**, 177 (1976).
- [43] P. Blaha, D. J. Singh, P. I. Sorantin, and K. Schwarz, Electric-field-gradient calculations for systems with large extended-core-state contributions, *Physical Review B* **46**, 1321 (1992).
- [44] P. T. Edwards, L. K. Saunders, D. C. Grinter, P. Ferrer, G. Held, E. J. Shotton, and S. L. M. Schroeder, Determination of H-atom positions in organic crystal structures by nexafs combined with density functional theory: a study of two-component systems containing isonicotinamide, *The Journal of Physical Chemistry A* **126**, 2889 (2022).
- [45] F. Iwase, K. Miyagawa, S. Fujiyama, K. Kanoda, S. Horiuchi, and Y. Tokura, Neutral-Ionic Phase Transition in DM-TTF-QCl₄ Investigated by ³⁵Cl NQR, *Journal of the Physical Society of Japan* **76**, 073701 (2007).
- [46] T. Kobayashi, Q.-P. Ding, H. Taniguchi, K. Satoh, A. Kawamoto, and Y. Furukawa, Charge disproportionation in the spin-liquid candidate κ -(ET)₂Cu₂(CN)₃ at 6 K revealed by ⁶³Cu NQR measurements, *Physical Review Research* **2**, 042023(R) (2020).
- [47] A. A. Abragam, *The Principles of Nuclear Magnetism* (Oxford University Press, Oxford, 1961).
- [48] S. Imajo, private communication.
- [49] M. Klanjšek, A. Zorko, R. Žitko, J. Mravlje, Z. Jagličić, P. K. Biswas, P. Prelovšek, D. Mihailovic, and D. Arčon, A high-temperature quantum spin liquid with polaron spins, *Nature Physics* **13**, 1130 (2017).
- [50] G. Wortmann, E. Bychkov, and Y. S. Grushko, ¹²⁹I-Mössbauer study of molecular dynamics in the organic superconductor β -(BEDT-TTF)₂I₃, *Hyperfine Interactions* **70**, 1179 (1992).
- [51] G. R. Stewart, J. O'Rourke, G. W. Crabtree, K. D. Carlson, H. H. Wang, J. M. Williams, F. Gross, and K. Andres, Specific heat of the ambient-pressure organic superconductor β -di[bis(ethylenedithio)tetrathiafulvalene] triiodide [β -(BEDT-TTF)₂I₃], *Physical Review B* **33**, 2046 (1986).
- [52] G. Grüner, The dynamics of charge-density waves, *Reviews of modern physics* **60**, 1129 (1988).
- [53] P. Matus, P. Bánki, and G. Kriza, ⁸⁷Rb NMR spin-lattice relaxation in the charge-density wave phase of Rb_{0.3}MoO₃, *Le Journal de Physique IV* **09**, Pr10 (1999).
- [54] T. Maniv, Effect of a spin density wave instability on the nuclear spin-lattice relaxation in quasi 1-*d* conductors, *Solid State Communications* **43**, 47 (1982).
- [55] T. Tsumuraya, H. Seo, and T. Miyazaki, First-Principles Study on the Stability and Electronic Structure of the Charge-Ordered Phase in α -(BEDT-TTF)₂I₃, *Crystals* **11**, 1109 (2021).

Supplementary Material:
**“Absence of hydrogen bonding in charge-ordered organic conductor
 α -(BEDT-TTF) $_2$ I $_3$ probed by $^{127}\text{I-NQR}$ ”**

T. Kobayashi,^{1,2,3,*} Y. Kato,¹ H. Taniguchi,¹ T. Tsumuraya,⁴ K. Hiraki,⁵ and S. Fujiyama³

¹*Graduate School of Science and Engineering, Saitama University, Saitama, 338-8570, Japan*

²*Research and Development Bureau, Saitama University, Saitama 338-8570, Japan*

³*Meson Science Laboratory, RIKEN, Saitama 351-0198, Japan*

⁴*POIE, Kumamoto University, Kumamoto 860-8555, Japan*

⁵*Center for Integrated Science and Humanities, Fukushima Medical University, Fukushima, 960-1295, Japan*

(Dated: August 15, 2022)

A. 1. Calculation of electric field gradients from first principles

All nuclei with a nuclear spin quantum number $I \geq 1$ have an electric quadrupole moment Q , which originated from the nonspherical charge distribution. The nuclear quadrupole interaction between Q and the electric-field gradients (EFG) at the nuclei position determines the coupling constant. EFG is very sensitive to the deviation of charge from the spherical part of potentials.

We performed a first-principles density-functional theory (DFT) calculation to compute EFG in α -(BEDT-TTF) $_2$ I $_3$ using the all-electron full-potential linearized augmented plane wave (FLAPW) method [1, 2]. In the EFG calculation, we refer to the experimental crystal structures above and below the charge ordering (CO) transition temperature $T_{\text{CO}} \approx 135$ K [3]. The EFG is usually very sensitive to internal atomic coordinates. Therefore, we performed structural optimization for the hydrogen and iodine atom positions using the DFT calculations. For the H-atom position, the x-ray diffraction relies on electron density at the scattering sites, and hydrogen atoms have low electron density [4]; C–H bond distances in the structures determined by x-ray diffraction is generally shorter than those optimized with DFT method.

The low-temperature structure is a triclinic structure with the space group of $P1$, which was measured at 30 K. Above the CO temperature, we used a centrosymmetric structure with the space group of $P\bar{1}$, measured at 150 K. Those structures were obtained with synchrotron x-ray diffraction [3]. The CIF (crystallographic information framework) files are deposited in the Cambridge structure database (Nos. 208980 and 208981).

In Table S1, we list the calculated EFG at the terminal iodine sites. The NQR frequencies ν_{Q} were obtained from these results and $\nu_{\text{Q}} = \frac{3eQV_{zz}}{20h} (1 + \frac{59}{54}\eta^2)$ with $Q = -680(10)$ mb [5], and are summarized in Table S2 along with the experimental values.

In the present DFT calculations, the Kohn–Sham equations are self-consistently solved using the FLAPW method implemented in the QMD-FLAPW code [1]. The exchange-correlation functional used is the generalized gradient approximation proposed by Perdew, Burke, and Ernzerhof [6]. The dimensions of the \mathbf{k} -point mesh used were $4 \times 4 \times 2$ for the self-consistent loop. The cutoff energies for the LAPW basis and the potential and density were 20.3 and 213.1 Ry, respectively. We set the muffin-tin (MT) sphere radii as 1.26, 0.75, 1.98, and 2.76 Bohr for C, H, S, and I atoms, respectively. The electronic states up to C ($2s$) 2 , S ($2p$) 6 , and I ($4d$) 10 were treated as core electrons, which are predominantly confined to the MT spheres.

TABLE S1. The principal values of the EFG tensor V_{zz} and asymmetry parameter η .

	D			E		
	$V_{zz}(10^{21}\text{V/m}^2)$	η	site	$V_{zz}(10^{21}\text{V/m}^2)$	η	site
150 K ($T > T_{\text{CO}}$)	70.533	0.036	I1(=I3)	70.152	0.043	I2(=I4)
30 K ($T < T_{\text{CO}}$)	70.897	0.036	I1	69.981	0.042	I2
	70.375	0.034	I3	69.848	0.043	I4

* tkobayashi@phy.saitama-u.ac.jp

TABLE S2. NQR frequencies of experiments (ν_Q^{exp}) and calculation (ν_Q^{cal}) for terminal iodines of I_3 anions.

	D			E		
	ν_Q^{exp} (MHz)	ν_Q^{cal} (MHz)	site	ν_Q^{exp} (MHz)	ν_Q^{cal} (MHz)	site
150 K ($T > T_{\text{CO}}$)	173.10	174.0	I1(=I3)	172.17	173.3	I2(=I4)
30 K ($T < T_{\text{CO}}$)	175.40	175.2	I1	173.04	172.9	I2
	172.38	173.8	I3	173.00	172.6	I4

-
- [1] E. Wimmer, H. Krakauer, M. Weinert, and A. J. Freeman, Full-potential self-consistent linearized-augmented-plane-wave method for calculating the electronic structure of molecules and surfaces: O_2 molecule, *Physical Review B* **24**, 864 (1981).
- [2] J. Yu, A. J. Freeman, R. Podloucky, P. Herzig, and P. Weinberger, Origin of electric-field gradients in high-temperature superconductors: $\text{YBa}_2\text{Cu}_3\text{O}_7$, *Physical Review B* **43**, 532 (1991).
- [3] S. Kitou, T. Tsumuraya, H. Sawahata, F. Ishii, K.-i. Hiraki, T. Nakamura, N. Katayama, and H. Sawa, Ambient-pressure Dirac electron system in the quasi-two-dimensional molecular conductor α -(BETS) $_2\text{I}_3$, *Physical Review B* **103**, 035135 (2021).
- [4] P. T. Edwards, L. K. Saunders, D. C. Grinter, P. Ferrer, G. Held, E. J. Shotton, and S. L. M. Schroeder, Determination of H-atom positions in organic crystal structures by nexafs combined with density functional theory: a study of two-component systems containing isonicotinamide, *The Journal of Physical Chemistry A* **126**, 2889 (2022).
- [5] H. Yakobi, E. Eliav, L. Visscher, and U. Kaldor, High-accuracy calculation of nuclear quadrupole moments of atomic halogens, *The Journal of Chemical Physics* **126**, 054301 (2007).
- [6] J. P. Perdew, K. Burke, and M. Ernzerhof, Generalized Gradient Approximation Made Simple, *Physical Review Letters* **77**, 3865 (1996).